Supporting Information

Enhanced Electrocatalytic Hydrogen Evolution in Alkaline Saline

Electrolyte by NiCo Foam Supported Iridium Nanoclusters

Jiaxin Yuan[1], Jinsong Zhou[1], Zehua Peng[1,2], Gang Li[1], Yang Hou[3], Michael K.H. Leung [1,4]

1 Ability R&D Energy Research Centre, School of Energy and Environment, City University of Hong Kong, Hong Kong, China;

2 Department of Mechanical Engineering, College of Engineering, City University of Hong Kong, Hong Kong, China;

3 Key Laboratory of Biomass Chemical Engineering of Ministry of Education, College of Chemical and Biological Engineering, Zhejiang University, Hangzhou 310027, China

4 State Key Laboratory of Marine Pollution, City University of Hong Kong, Hong Kong, China.

*Corresponding author
Email: mkh.leung@cityu.edu.hk

Material and methods

1.1 Catalyst Preparation

Preparation of Ir-nc@m-NiCo.

Commercial NiCo foam was immersed in 1.0 M HCl, acetone, ethanol, and deionized water for 10 min in an ultrasonic machine, respectively. After treatments, three pieces of NiCo foams were dipped into 10 mM of $IrCl_3 \cdot 3H_2O$ solution for 24 hours and dehydrated at room temperature. The loading amount of Ir-nc@ m-NiCo catalyst was ~ 0.2 mg cm^{-2}.

Preparation of Ir-nc@Ni.

Commercial Ni foam was immersed in 1.0 M HCl, acetone, ethanol, and deionized water for 10 min in an ultrasonic machine, respectively. After treatments, three pieces of Ni foams were dipped into 10 mM of $IrCl_3 \cdot 3H_2O$ solution for 24 hours and dehydrated at room temperature.

Preparation of Ir-nc@Co.

Commercial Co foam was immersed into 1.0 M HCl, acetone, ethanol, and deionized water for 10 min in an ultrasonic machine, respectively. After treatments, three pieces of Co foams were dipped into 10 mM of $IrCl_3 \cdot 3H_2O$ solution for 24 hours and dehydrated at room temperature.

Preparation of NiCoIr-2.5, NiCoIr-5, and NiCoIr-20.

The prepared NiCo foams were separately dipped into 2.5, 5, and 20 mM of $IrCl_3 \cdot 3H_2O$ solution for 24 hours and dehydrated at room temperature.

Preparation of Pt@NiCo.

Commercial NiCo foam was immersed in 1.0 M HCl, acetone, ethanol, and deionized water for 10 min in an ultrasonic machine. After treatments, three NiCo Co foams were dipped into 10 mM of $PtCl_2$ solution for 24 hours and dehydrated at room temperature.

Preparation of Pt/C@NiCo, Ir/C@NiCo

A mixture of 0.4 mg of Ir/C, 810 μL of Nafion (5%), and 90 μL of ethanol was ultrasonicated for 30 min, then oscillated to obtain uniform dispersion. After the Pt/C dispersion was dropped onto the treated NiCo foam, the Pt/C@NiCo was gradually dried in a fume hood. The loading amount of Ir/C was ~ 0.2 mg cm^{-2}. A similar procedure was used to prepare Ir/C@NiCo.

1.2. Physical characterization

The morphologies and microstructures of the samples were surveyed by field-emission scanning electron microscopy (FESEM, Tescan MIRA LMS), and transmission electron microscopy (TEM) measurements performed on a FEI Tecnai F20 electron microscope with an expediting voltage of 200 kV. RIGAKU D/MAX 2550/PC (RIGAKU D/MAX 2550/PC) can obtain X-ray diffraction patterns (XRD). X-ray photoelectron spectroscopy (XPS, Thermo Scientific K-Alpha) used Al Kα radiation with 1486.6 eV.

1.3. Electrochemical measurements

The electrochemical tests were performed in a three-electrode cell using 1.0 M KOH as an electrolyte. The Ir nc@m-NiCo electrode, a Pt electrode, and an Ag/AgCl electrode served as the working, counter, and reference electrodes, respectively. Mechanical robustness and stability were studied through the multiple-current steps, multiple-potential steps, and amperometry current-time measurements. The electrochemical measurements were performed after stabilizing cyclic voltammetry (CV) cycles. Linear sweep voltammetry (LSV) can acquire the HER catalytic activity with a scan rate of 5 mV s^{-1}. The CV tests assessed the electrochemical double-layer capacitance at various scan rates from 20 to 100 mV s^{-1}. To ascertain the double-layer capacitance (C_{dl}), the CV scans between 0.29 and 0.39 V (vs. Ag/AgCl) were conducted at 100, 120, 140, 160, and 180 mV s^{-1}. The potentials vs. RHE in 1.0 M at 25 °C could be calculated through the original Nernst equation:

$E_{RHE} = E_{Ag/AgCl} + 0.0591$ pH $+0.098$ V.

1.4 DFT Calculation:

To obtain more insight into the mechanism of HER activity of Ir nc@m-NiCo. We have employed the Vienna Ab initio Simulation Package (VASP) to perform all density functional theory (DFT) calculations within the generalized gradient approximation (GGA) using the Perdew-Burke-Ernzerhof (PBE) functional. We have chosen the projected augmented wave (PAW) potentials to describe the ionic cores and take valence electrons into account using a plane wave basis set with a kinetic energy cutoff of 400 eV. The DFT-D3 empirical correction method was employed to describe van der Waals interactions. Geometry optimizations were performed with the force convergency smaller than 0.05 eV/Å. Monkhorst-Pack k-points of 1×1×1 were applied for all the calculations. The bottom layer atoms at the bottom are fixed in all the calculations. The free energy changes (ΔG) of each elementary reaction step during HER were calculated using the computational hydrogen electrode (CHE) model. In this model, the chemical potential is equal to the energy of half of the gas-phase H_2 at 0 V vs reversible hydrogen electrode (RHE). The electrode potential, U versus RHE, is considered by adding -eU when an electron transforming step occurs. That is

$G(U) = G(0 \text{ V}) - neU$, where e is the elementary charge of an electron, n is the number of proton-electron pairs transferred, and U is the applied potential. The following equation calculated the Gibbs free energy:

$$\Delta G^*H = E^*H - E_{surf} - (E_{H2})/2 + \Delta E_{ZPE} - T\Delta S$$

Where E^*H, E_{surf}, E_{H2}, ΔE_{ZPE}, and ΔS are the total energies of the slab with H-adsorbed surface, the clean surface, the isolated hydrogen molecule, the zero-point energy change, the entropy change at 300K, respectively.
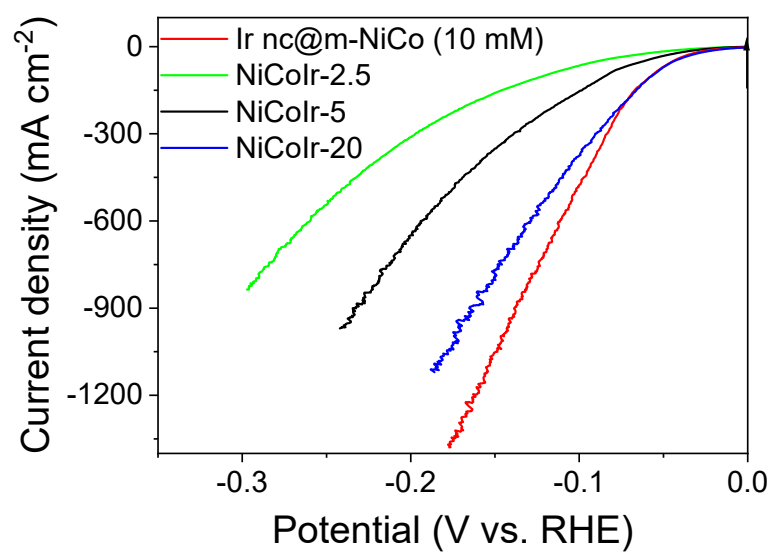
Figure S1 Polarization curves of Ir-nc@m-NiCo (10 mM), NiCoIr-2.5, NiCoIr-5, and NiCoIr-20.
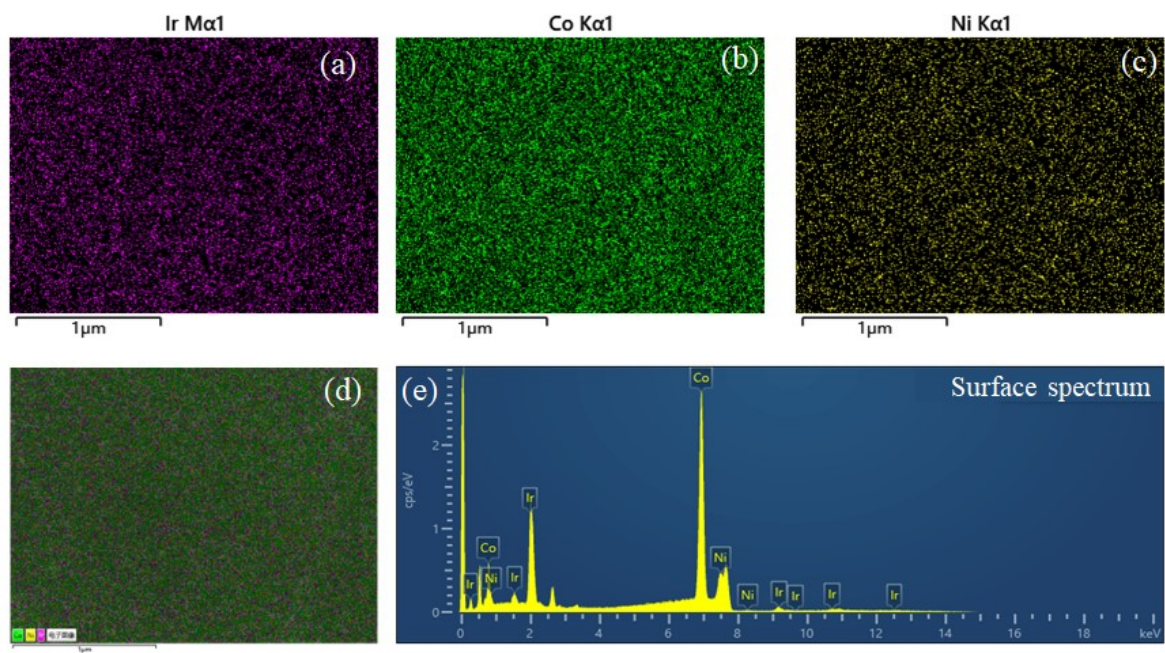
Figure S2. STEM-EDX mapping and spectrum of Ir-nc@m-NiCo.
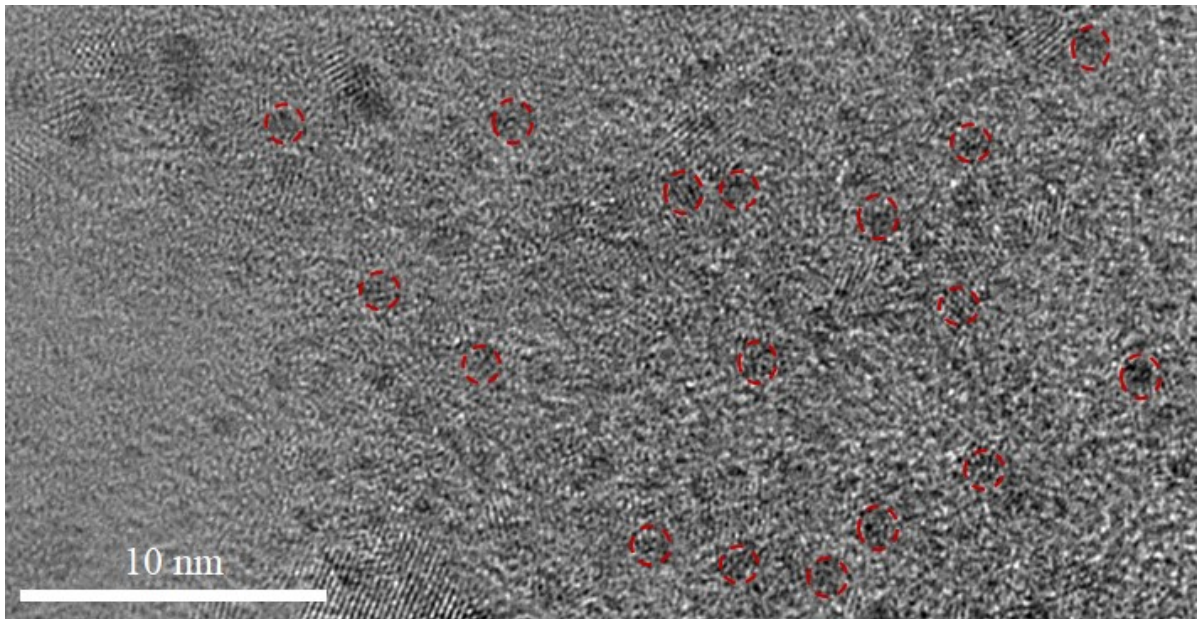
Red circles indicate Ir nanoclusters

Figure S3. HR-TEM images of Ir-nc@m-NiCo.
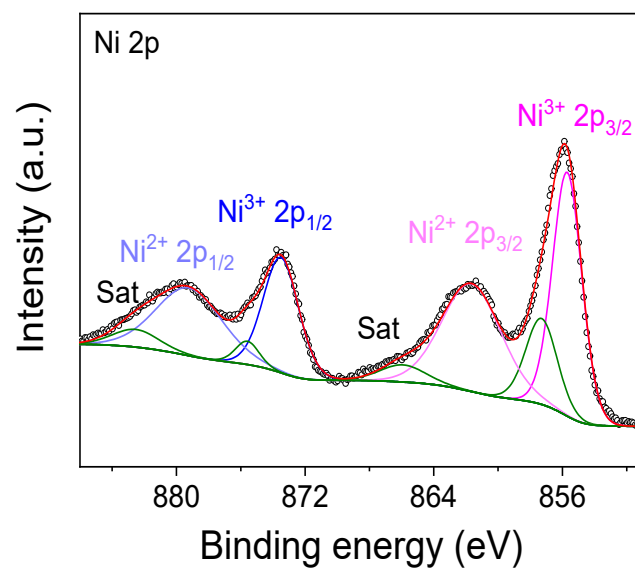
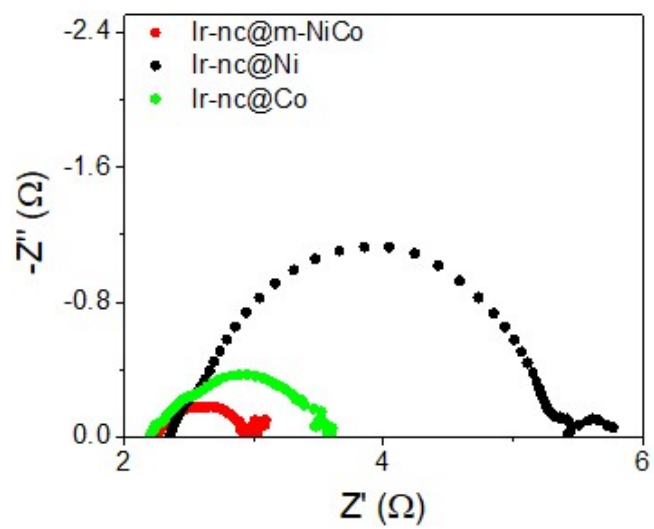Figure S4. High-resolution XPS spectra of Ni 2p of Ir-nc@Ni.

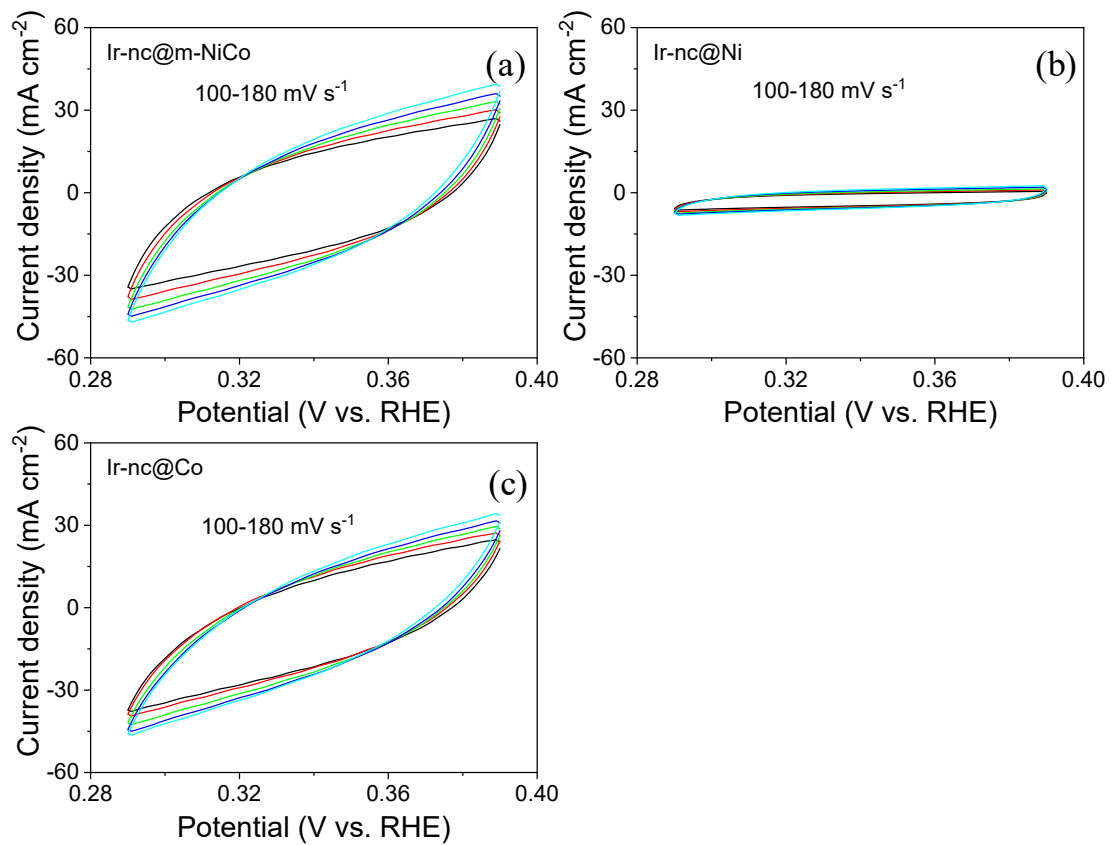Figure S5. Nyquist plots of Ir-nc@m-NiCo, Ir-nc@Ni, and Ir-nc@Co.

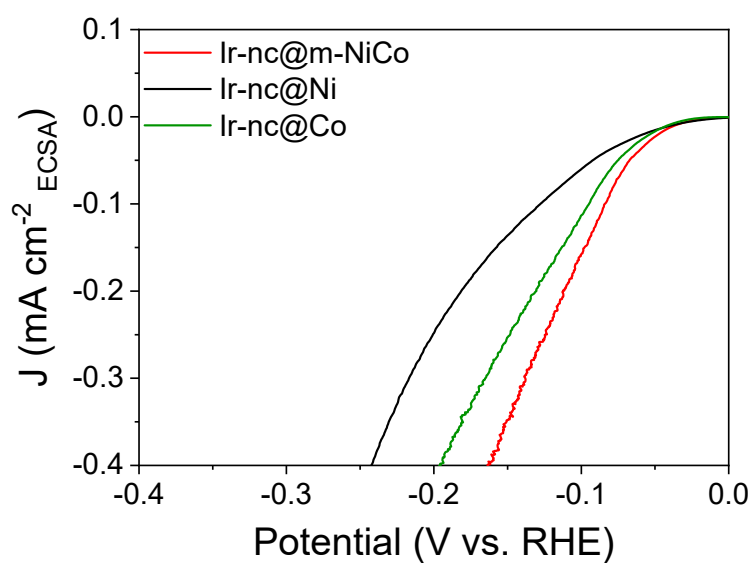Figure S6. ECSAs of Ir-nc@m-NiCo, Ir-nc@Ni, and Ir-nc@Co for HER in 1.0 M KOH electrolytes.

Figure S7. ECSA-normalized polarization curves of Ir-nc@m-NiCo, Ir-nc@Ni, and Ir-nc@Co for HER in 1.0 M KOH electrolytes.
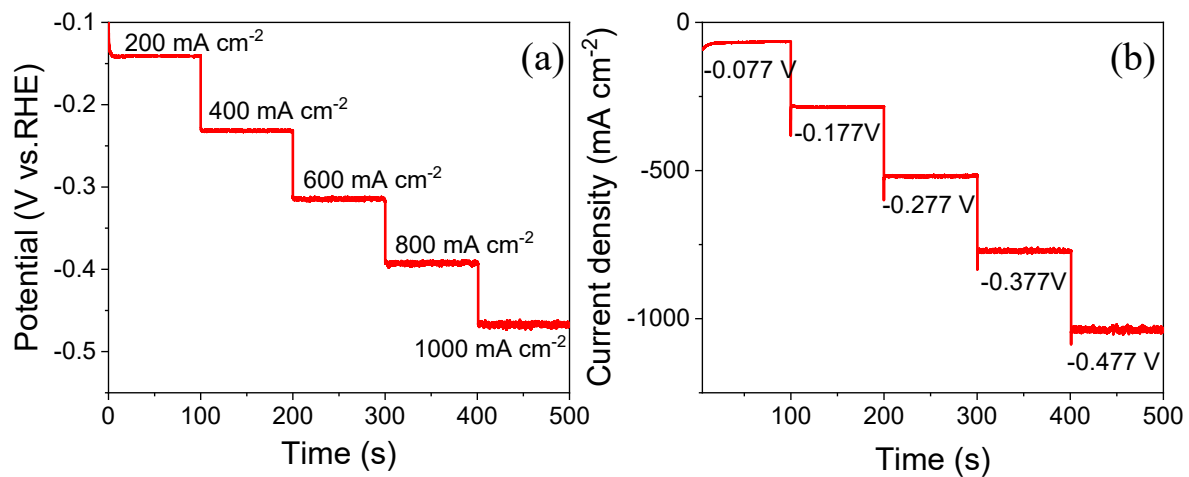
Figure S8. (a–b) Multi-current and multi-potential steps curves for Ir-nc@m-NiCo (without iR compensation).
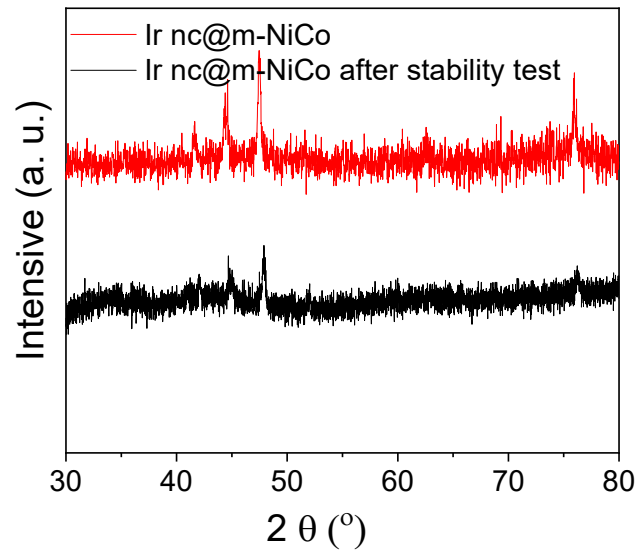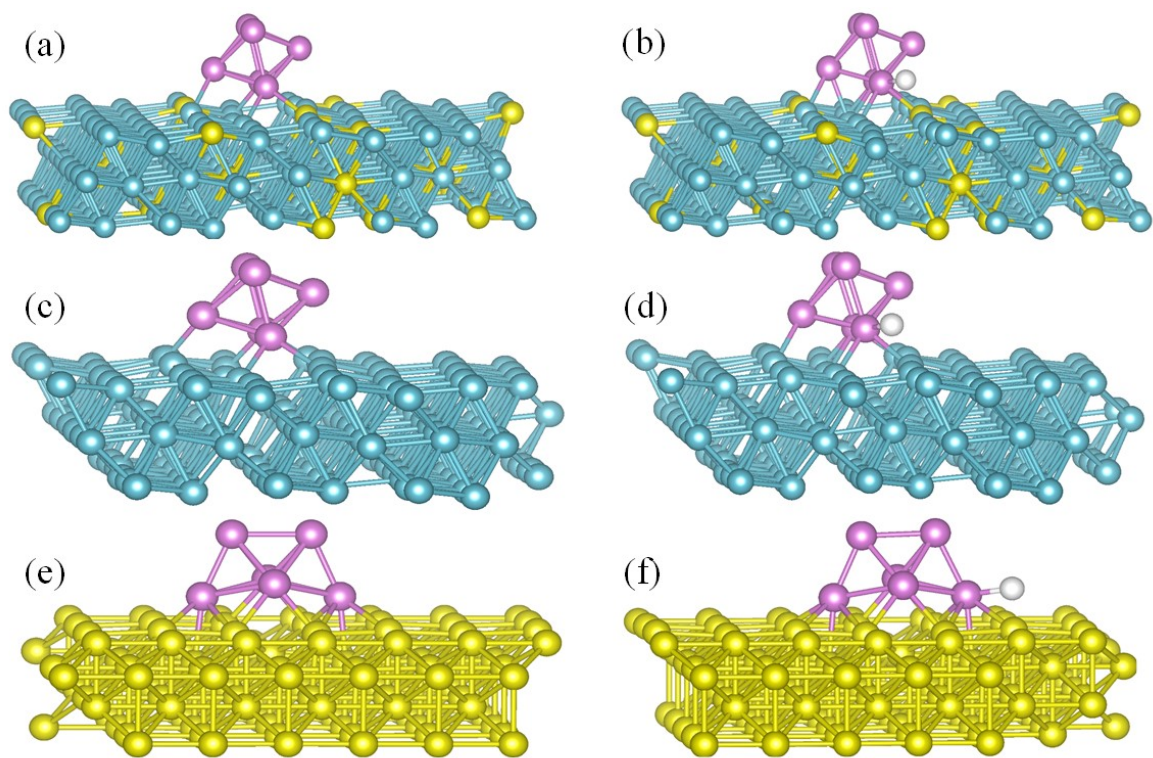
Figure S9. XRD of Ir-nc@m-NiCo after stability test.

Figure S10. Theoretical calculations of the hydrogen adsorption configured for NiCoIr (a–b), CoIr (c–d), and NiIr (e–f).
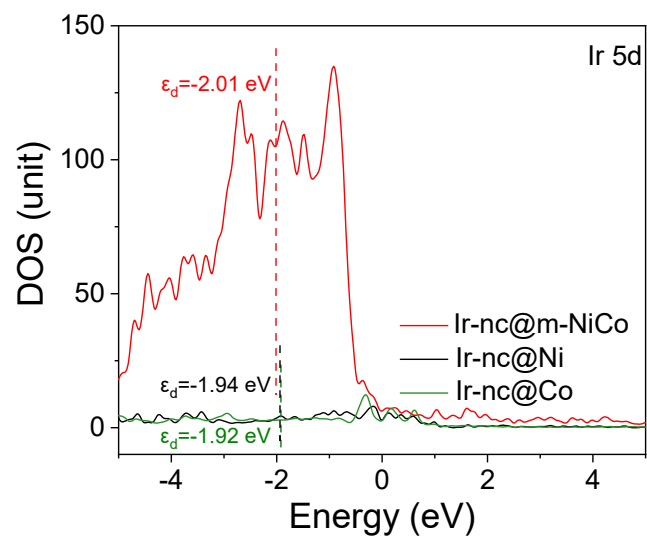
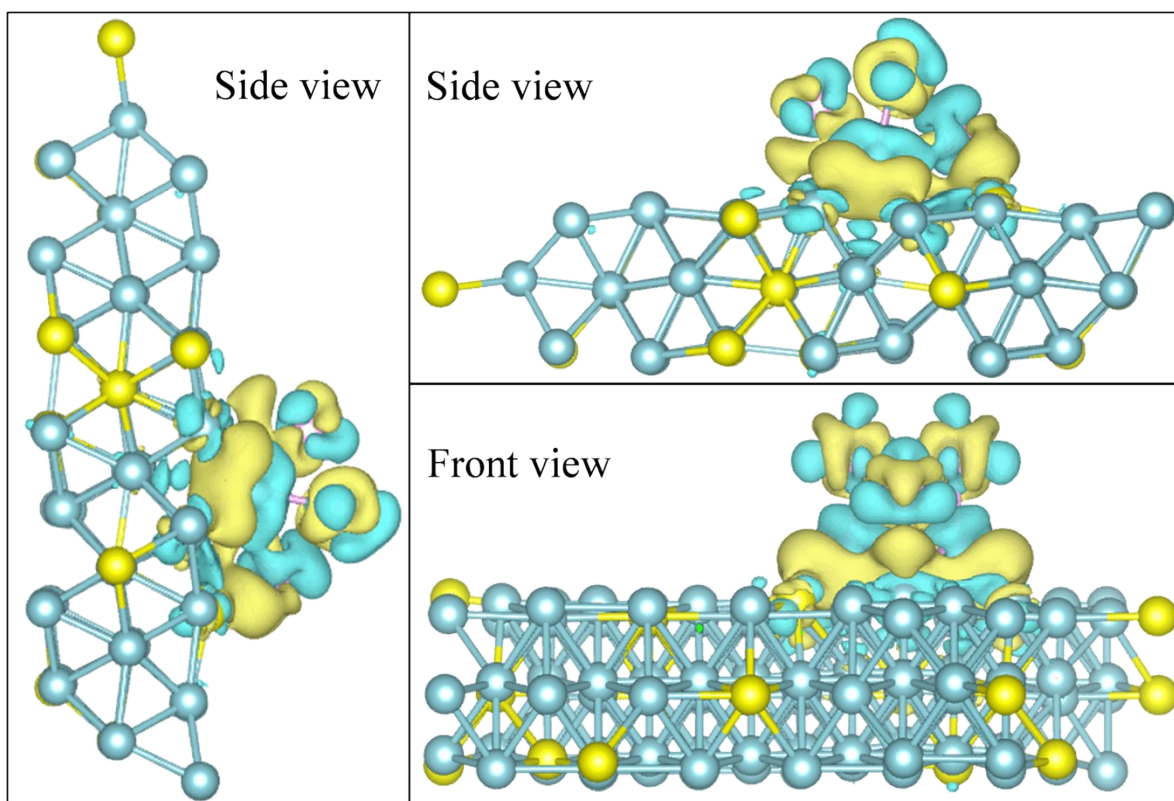Figure S11. Calculated DOS of Ir in Ir-nc@m-NiCo, Ir-nc@Ni, and Ir-nc@Co.

Figure S12. Charge density of Ir-nc@m-NiCo (side view and front view). Yellow represents the electron accumulation area, and blue represents the electron dissipation area.
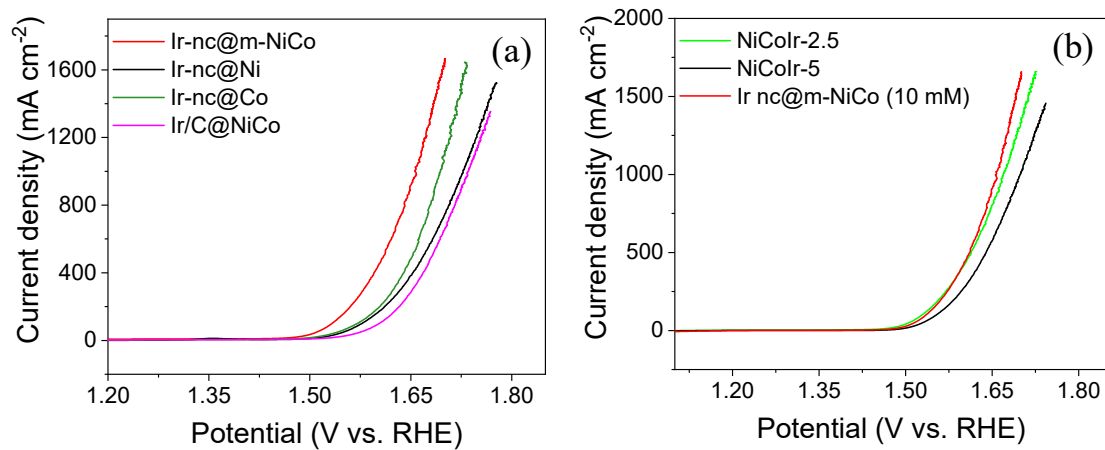
Figure S13. (a) Polarization curves of Ir-nc@m-NiCo, Ir-nc@Ni, Ir-nc@Co, and Ir/C@NiCo; (b) Polarization curves of Ir-nc@m-NiCo (10 mM), NiCoIr-2.5, and NiCoIr-5.
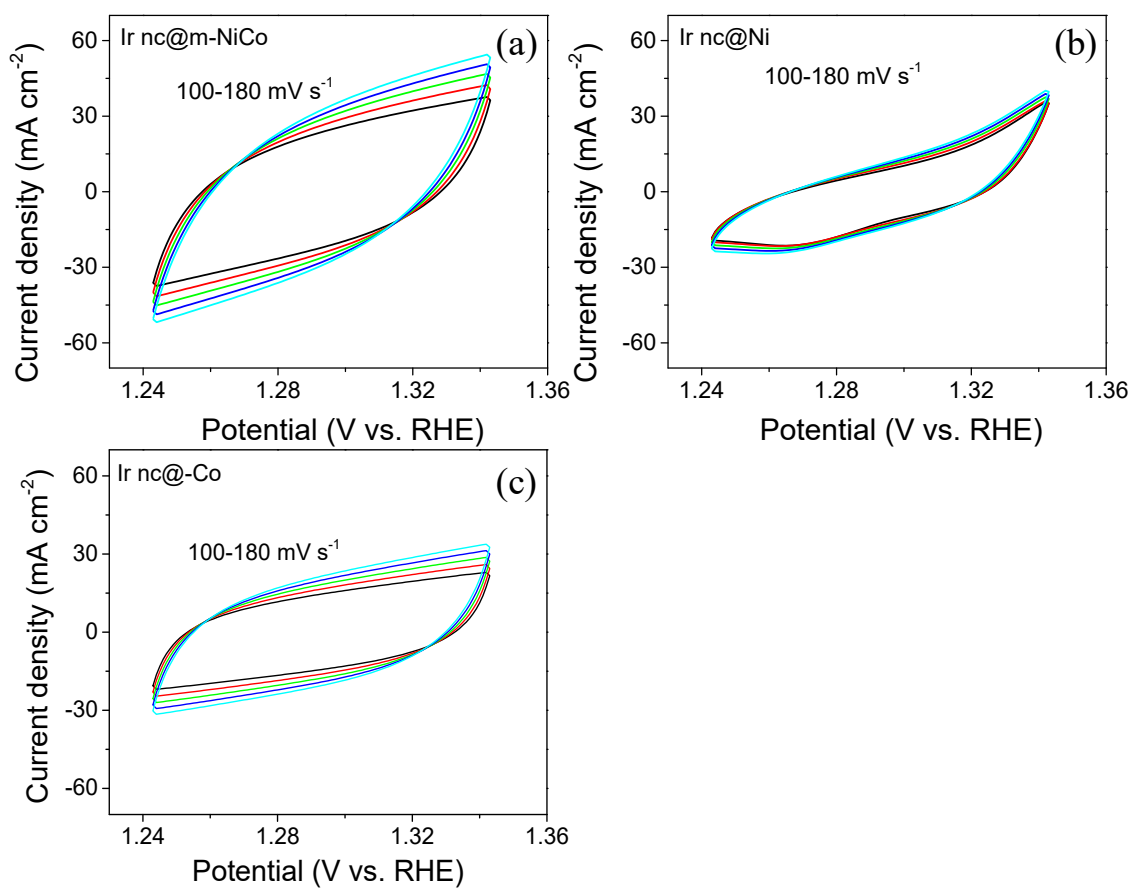
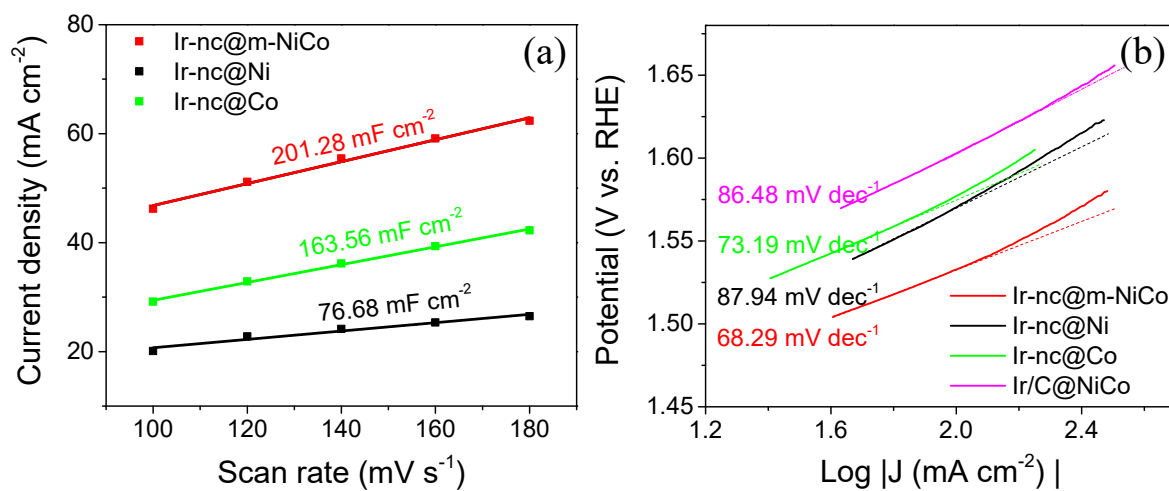Figure S14. (a–c) ECSAs of Ir-nc@m-NiCo, Ir-nc@Ni, and Ir-nc@Co for OER.

Figure S15. The corresponding ECSAs and Tafel plots of Ir-nc@m-NiCo, Ir-nc@Co, Ir-nc@Ni, and Ir/C@NiCo for OER.
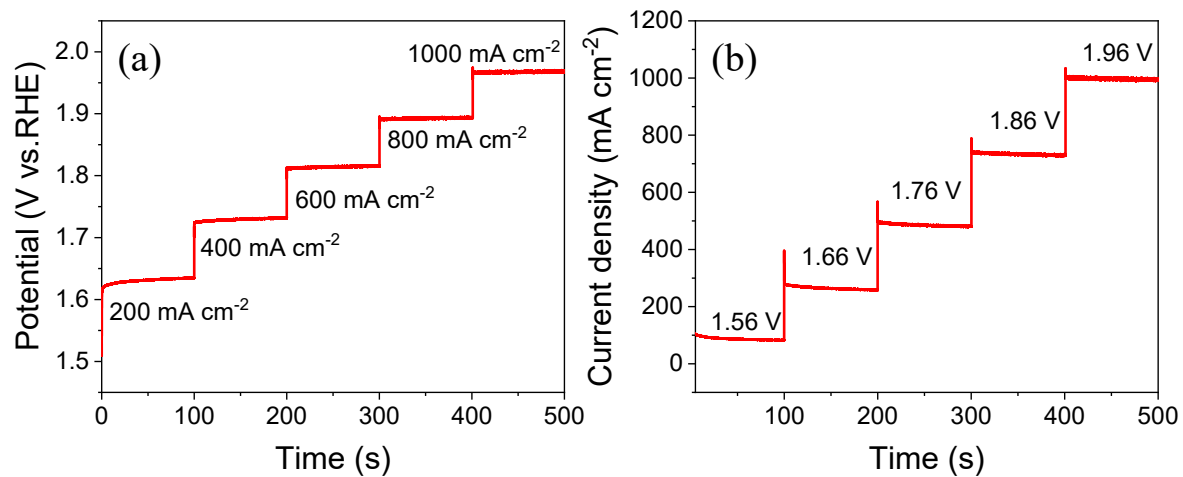
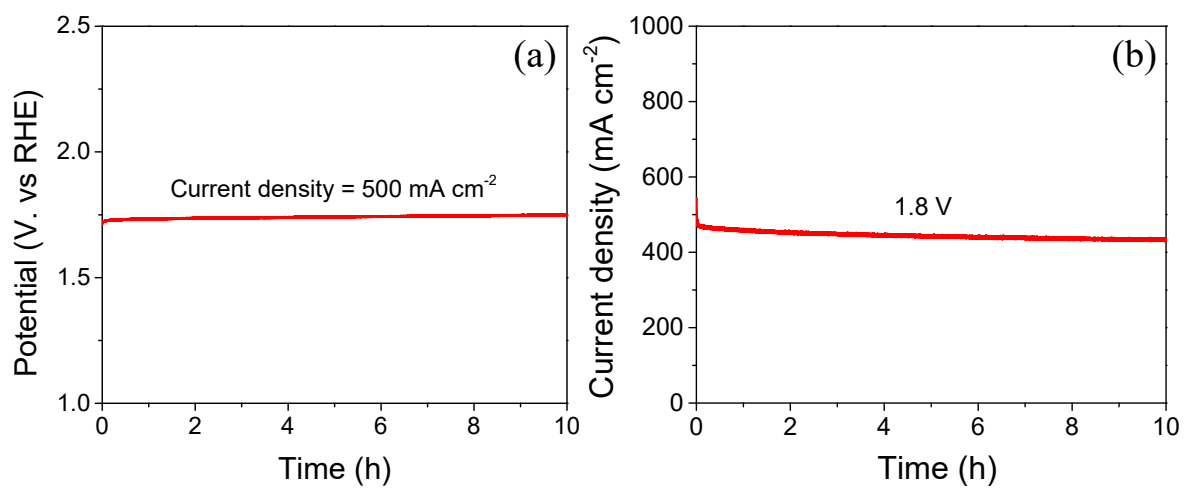Figure S16. (a–b) Multi-current steps curve and multi-potential steps curve for Ir-nc@m-NiCo.

Figure S17. (a-b) Chronopotentiometry and chronoamperometry curve with the Ir-nc@m-NiCo as the electrode at 500 mA cm^{-2}，and 1.8 V without iR compensation.
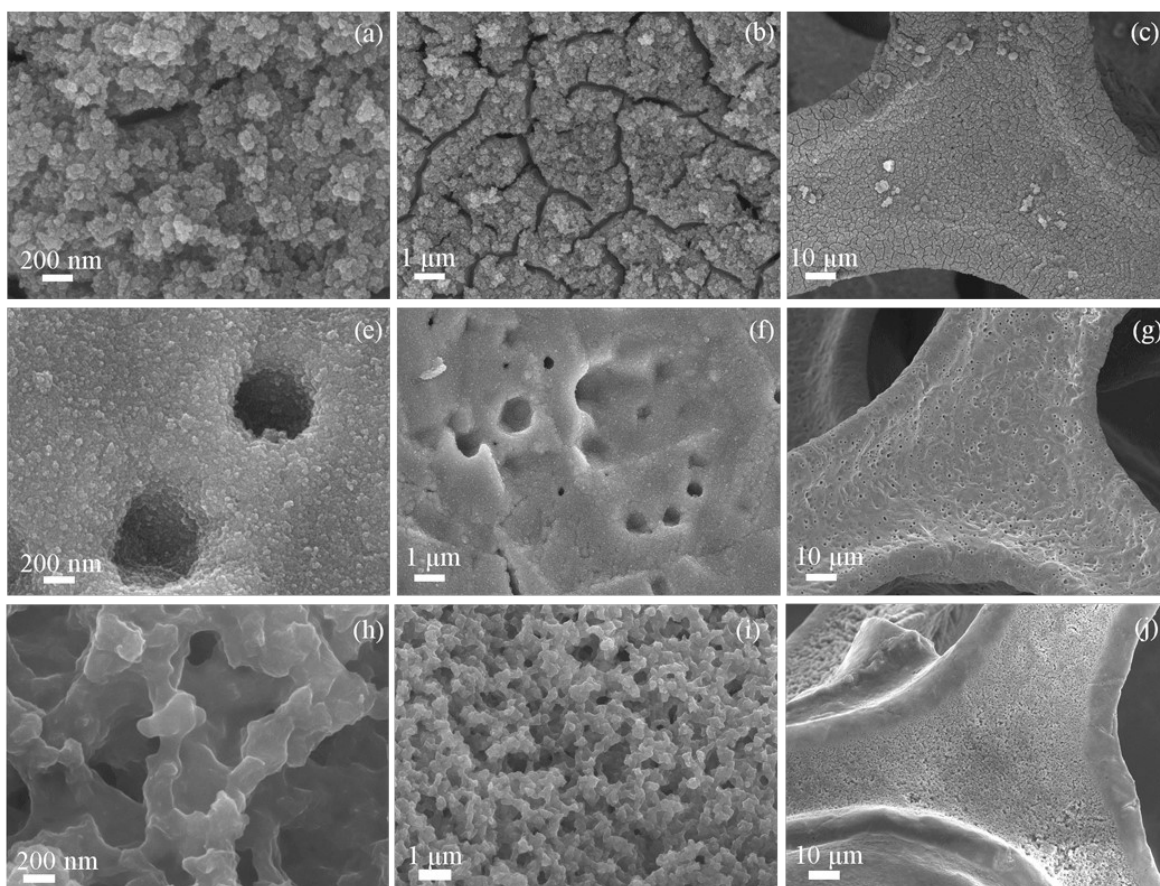
Figure S18. (a–c) FESEM images of NiCoIr-2.5, (e–g) FESEM images of NiCoIr-5, (h–j) FESEM images of NiCoIr-20.

Furthermore, the morphologies of Ir-nc@m-NiCo were characterized using FE-SEM. When NiCo foam is immersed in $IrCl_3·3H_2O$ solution with a concentration of 2.5 mM, the NiCo foam will generate surface cracks due to corrosion effects, and a layer of nanoparticles will grow in situ. Upcoming increasing the solution concentration to 5 mM, the cleavage layer on the nickel-cobalt surface detaches, and iridium nanoclusters and macropores of various sizes grew on the surface of the NiCo skeleton. With a further increase in the solution concentration to 10 mM, the amount of nanocluster growth begins to increase. The morphology transforms to nanoparticles when the concentration is raised to 20 mM. This transformation is attributed to the highly concentrated solution, which leads to violent corrosion of the nickel-cobalt foam and results in the growth of Ir nanoparticles on the surface.
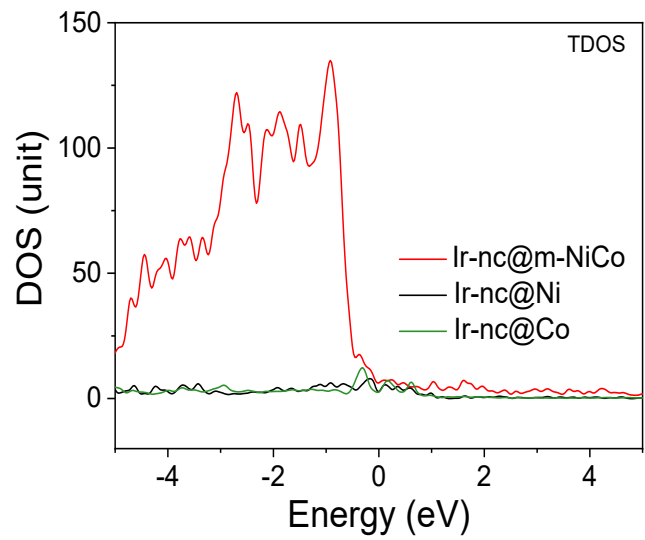
Figure S19. The calculated density of total states graphs of Ir-nc@m-NiCo, Ir-nc@Co, and Ir-nc@Ni.

Figure S20 Polarization curves of Ir-nc@m-NiCo, Pt@NiCo, and Pt@NiCo.

Figure S21. ECSA-normalized polarization curves of Ir-nc@m-NiCo, Ir-nc@Ni, and Ir-nc@Co for HER in 1.0 M KOH and 0.5 M NaCl electrolytes.

Figure S22. ECSAs of Ir-nc@m-NiCo, Ir-nc@Ni, and Ir-nc@Co for HER in 1.0 M KOH and 0.5 M NaCl electrolytes.

Figure S23. ECSAs of Ir-nc@m-NiCo, Ir-nc@Ni, and Ir-nc@Co in 1.0 M KOH and 0.5 M NaCl electrolytes.

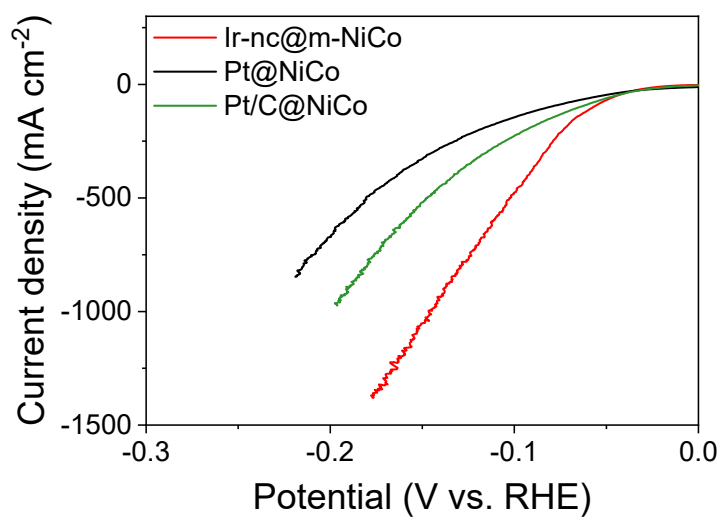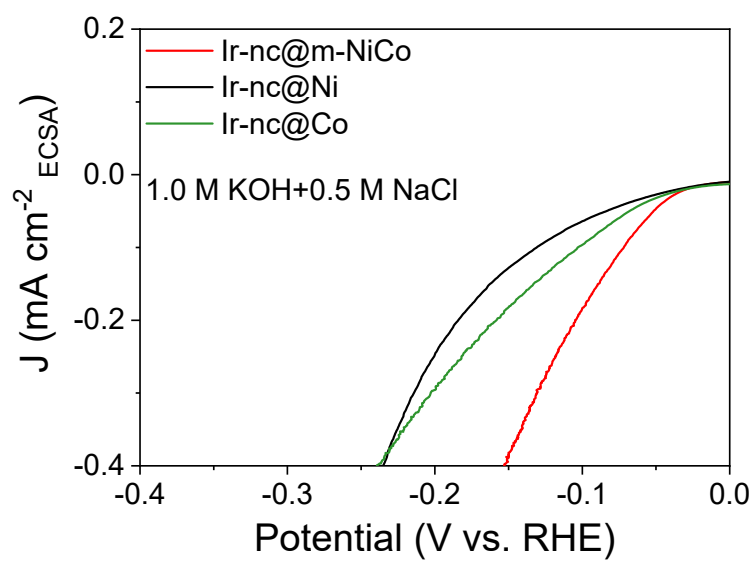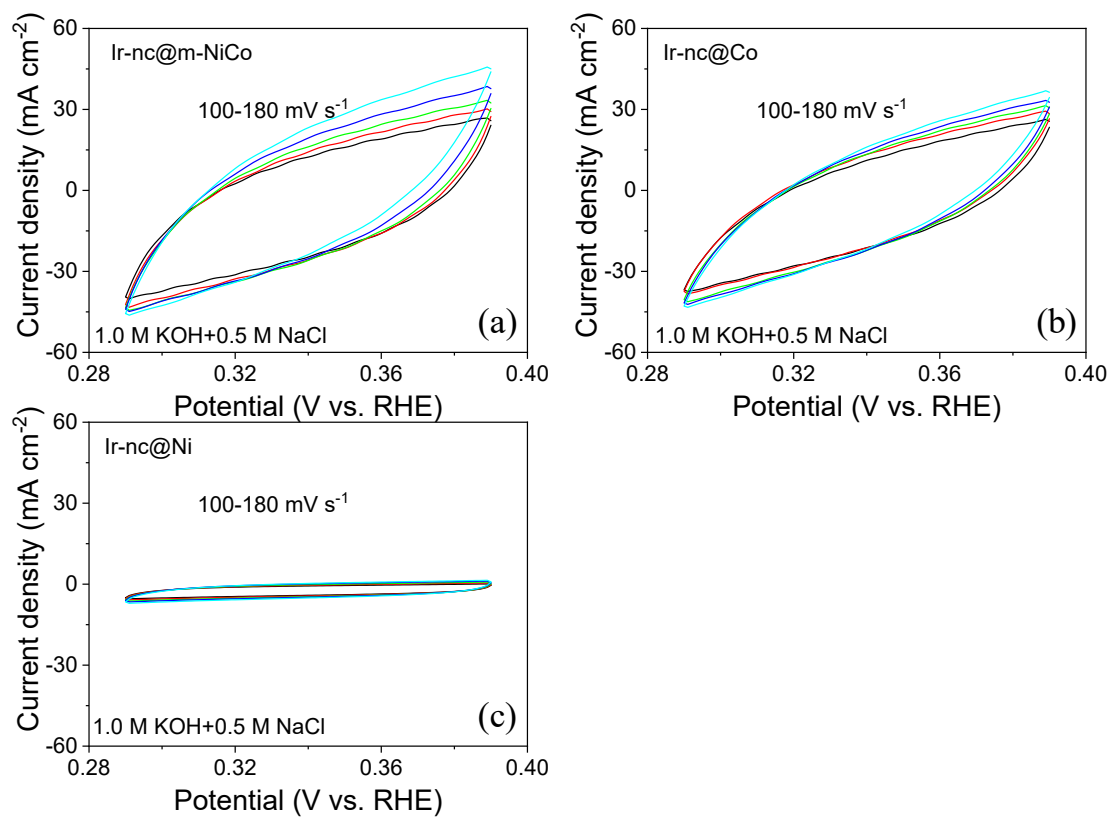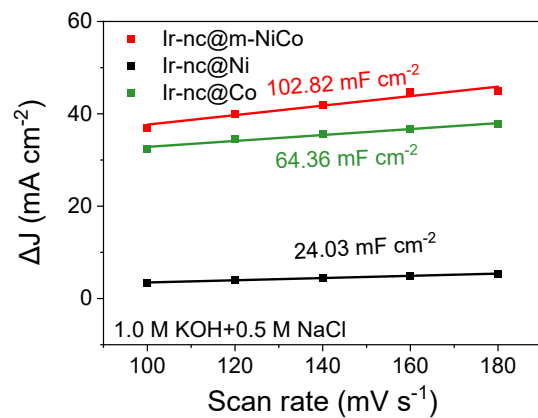**Table S1.** HER activities of representative benchmark electrocatalysts in alkaline solution in terms of the potential to achieve the 100, 500, and 1,000 mA cm^{-2}.

Material	Electrolyte	Substrate	Tafel slope (mV dec^{-1})	-10 mA cm^{-2}	-100 mA cm^{-2}	-500 mA cm^{-2}	-1,000 mA cm^{-2}	Ref.
Ir-nc@m-NiCo	**1.0 M KOH**	**NiCo**	**30.8**	20.8	**59**	**101**	**146**	**this work**
Ru-NiCoP/NF	1.0 M KOH	NF	**45.4**	44	103	-	-	[1]
FeIr/NF	1.0 M KOH	NF	**50.46**	25.6	70	246	327	[2]
RuCoP/CC	1.0 M KOH	CC	**75**	58	100	-	-	[3]
Ir-NiCo LDH	1.0 M KOH	NF	**33.2**	21	80	-	-	[4]
Pt/Ni(OH)$_2$/NF-A	1.0 M KOH	NF	**37.6**	25.3	211	-	-	[5]
Ru/c-Ti$_3$C$_2$T$_x$/NF	1.0 M KOH	NF	**60**	37	113	219-	320	[6]
CC@WS$_2$/ Ru-450	1.0 M KOH	CC	**53.2**	32.1	110	-	-	[7]
Ru-NiFeP/NF	1.0 M KOH	NF	**67.8**	29	139.5	-	-	[8]
IrNi-FeNi$_3$/NF	1.0 M KOH	NF	**66.9**	31.1	138.9	248.6	413.2	[9]
Ru$_1$CoP/CDs	1.0 M KOH	CDs	**74.5**	51	340	-	-	[10]

1.   Chen, D.; Lu, R.; Pu, Z.; Zhu, J.; Li, H.-W.; Liu, F.; Hu, S.; Luo, X.; Wu, J.; Zhao, Y.; Mu, S., Ru-doped 3D flower-like bimetallic phosphide with a climbing effect on overall water splitting. *Applied Catalysis B: Environmental* **2020,** *279*, 119396.

2.   Chen, J.; Wang, Y.; Qian, G.; Yu, T.; Wang, Z.; Luo, L.; Shen, F.; Yin, S., In situ growth of volcano-like FeIr alloy on nickel foam as efficient bifunctional catalyst for overall water splitting at high current density. *Chemical Engineering Journal* **2021,** *421*, 129892.

3.   Chen, Y.; Wang, D.; Meng, T.; Xing, Z.; Yang, X., Modulating the Electronic Structure by Ruthenium Doping Endows Cobalt Phosphide Nanowires with Enhanced Alkaline Hydrogen Evolution Activity. *ACS Applied Energy Materials* **2022,** *5* (1), 697-704.

4.   Fan, R.; Mu, Q.; Wei, Z.; Peng, Y.; Shen, M., Atomic Ir-doped NiCo layered double hydroxide as a bifunctional electrocatalyst for highly efficient and durable water splitting. *Journal of Materials Chemistry A* **2020,** *8* (19), 9871-9881.

5.   Gu, Y.; Wang, Y.; Shi, J.; Yang, M.; Rui, Y.; An, W.; Men, Y., Well-dispersed Pt nanodots interfaced with Ni(OH)2 on anodized nickel foam for efficient hydrogen evolution reaction. *International Journal of Hydrogen Energy* **2020,** *45* (51), 27067-27077.

6.   Kong, A.; Peng, M.; Gu, H.; Zhao, S.; Lv, Y.; Liu, M.; Sun, Y.; Dai, S.; Fu, Y.; Zhang, J.; Li, W., Synergetic control of Ru/MXene 3D electrode with superhydrophilicityandsuperaerophobicity for overall water splitting. *Chemical Engineering Journal* **2021,** *426*, 131234.

7.   Li, J.; Li, Y.; Wang, J.; Zhang, C.; Ma, H.; Zhu, C.; Fan, D.; Guo, Z.; Xu, M.; Wang, Y.; Ma, H., Elucidating the Critical Role of Ruthenium Single Atom Sites in Water Dissociation and Dehydrogenation Behaviors for Robust Hydrazine Oxidation-Boosted Alkaline Hydrogen Evolution. *Advanced Functional Materials* **2022,** *32* (16), 2109439.

8.   Lin, Y.; Zhang, M.; Zhao, L.; Wang, L.; Cao, D.; Gong, Y., Ru doped bimetallic phosphide derived from 2D metal organic framework as active and robust electrocatalyst for water splitting. *Applied Surface Science* **2021,** *536*, 147952.

9.   Wang, Y.; Qian, G.; Xu, Q.; Zhang, H.; Shen, F.; Luo, L.; Yin, S., Industrially promising IrNi-FeNi3 hybrid nanosheets for overall water splitting catalysis at large current density. *Applied Catalysis B: Environmental* **2021,** *286*, 119881.

10.   Song, H.; Wu, M.; Tang, Z.; Tse, J. S.; Yang, B.; Lu, S., Single Atom Ruthenium-Doped CoP/CDs Nanosheets via Splicing of Carbon-Dots for Robust Hydrogen Production. *Angewandte Chemie International Edition* **2021,** *60* (13), 7234-7244.